PCCP

RSC Publishing

COMMUNICATION

View Article Online
View Journal | View Issue

Protons crossing triple phase boundaries based on a metal catalyst, Pd or Ni, and barium zirconate†

Cite this: *Phys. Chem. Chem. Phys.*, 2013, **15**, 12525

Received 2nd May 2013,
Accepted 6th June 2013

DOI: 10.1039/c3cp51863a

www.rsc.org/pccp

Massimo Malagoli,[a] M. L. Liu,[b] Hyeon Cheol Park[c] and Angelo Bongiorno*[a]

Density functional theory calculations are used to investigate the energetics of protons crossing triple phase boundaries based on a metal catalyst, Pd or Ni, and barium zirconate. Our calculations show that the proton transfer reaction at these interfaces is controlled by the terminal layer of the electrolyte in contact with the metallic and gas phases. The hydrogen spilling process onto the electrolyte surface is energetically favored at peripheral sites of the metal–electrolyte interface, and proton incorporation into the sub-surface region of the electrolyte involves energies of the order of 1 eV. At the triple phase boundary, the energy cost associated with the proton transfer reaction is controlled by both the nature of chemical contact and the Schottky barrier at the metal–electrolyte interface.

Introduction

Triple phase boundaries (TPBs) are electrochemical "hot spots" in heterogeneous porous electrodes of fuel cells.[1] The concept of TPBs holds that key reaction steps governing fuel cell electrodes occur at confined spatial sites – called "triple phase boundaries" – where a metal catalyst, an electrolyte, and a gas phase come into contact.[2–6] While the current understanding of TPBs remains limited, the future of the fuel cell technology relies on new materials and solutions enhancing electrochemical performances. To this end, a basic understanding of TPBs needs to be achieved.[2–6] Here, we use density functional theory (DFT) calculations to investigate TPBs based on a metal and a proton conducting electrolyte, mimicking TPBs in the anode of proton ceramic fuel cells (PCFCs).[7,8]

In the anode of PCFCs, hydrogen or hydrocarbons split on the surface of a metallic catalyst. Hydrogen adsorbed on the metal surface migrates toward the TPBs, incorporates into the proton conducting ceramic, diffuses across the electrolyte, and finally reaches the cathode where it reacts with oxygen ions to form water molecules.[7,8] The current understanding of materials surfaces and interfaces, TPBs, and elementary processes in fuel cells is limited and a matter of significant interest.[9–12] Among the various efforts, computational modeling studies are becoming a useful means to elucidate – piece by piece – the electrochemical properties of these complex material systems. So far, the most notable computational efforts undertaken to study TPBs and go beyond phenomenological pictures are those of Shishkin and Ziegler[5,13] and Cucinotta *et al.*[6] These DFT studies considered TPBs based on Ni and yttria-stabilized zirconia (YSZ), and focused on reaction mechanisms leading to the formation of water molecules near these TPBs.[5,6]

In this work, we consider TPBs formed by either Pd or Ni and yttrium-doped barium zirconate (BZY), a proton conducting electrolyte forming a class of novel materials for a new generation of SOFCs, for hydrogen separation and purification, and for electrolysis of water.[14–16] Here, we investigate the energetics of the following key elementary process:

$$\mathrm{H^*[metal]} \rightarrow \mathrm{H^+[BZY]} + \mathrm{e}\ , \qquad (1)$$

leading to the transfer of a hydrogen species from the metallic to the electrolyte component of the TPB. Reaction (1) occurs at the interface between the metal and the electrolyte, and it involves an electron transfer step to an acceptor state near the TPB. Due to the complexity of interfacial TPB regions and the above "proton coupled electron transfer" reaction, the energetics of reaction (1) is addressed here by considering the situation of a lightly Y-doped electrolyte and a proton incorporation process accompanied by an electron transfer step to the metal component of the TPB. Further, due to the difficulty in modeling TPBs under operating conditions, in this work we disregard effects related to both concentration of protons and electrode polarization, and we focus on the energetics of reaction (1) occurring for a single and isolated H species at TPBs under open current voltage conditions. Under the aforementioned assumptions,

[a] *School of Chemistry & Biochemistry, Georgia Institute of Technology, Atlanta, Georgia 30332-0400, USA. E-mail: angelo.bongiorno@chemistry.gatech.edu*
[b] *School of Material Science & Engineering, Georgia Institute of Technology, Atlanta, Georgia 30332-0245, USA*
[c] *Advanced Materials Research Center, Samsung Advanced Institute of Technology (SAIT), San 14-1, Nongseo-dong, Yongin-si 446-712, Republic of Korea*

† Electronic supplementary information (ESI) available. See DOI: 10.1039/c3cp51863a

our study shows that reaction (1) is endothermic and involves energy costs ranging between a few tenths up to more than an eV, depending on where near a TPB the proton incorporates into the electrolyte. In proximity of the metallic catalysts, the activation energy of reaction (1) is controlled by the Schottky energy barrier at the metal–electrolyte interface and the occurrence of low-energy interfacial trap states. Far from the TPB, protons on the electrolyte surface can incorporate into the bulk by overcoming energy barriers larger than 1 eV. Overall, the basic insights reported in this computational study suggest routes to control the performance of TPBs and constitute the basis for addressing and elucidating the electrochemical performance of TPBs under operating conditions.

Methods

In this work, we use the Vienna *Ab initio* Simulation Package[17,18] to perform DFT calculations. In the case of $BaZrO_3$ (space group $Pm\bar{3}m$), this DFT scheme gives a lattice constant, bulk modulus, and static dielectric constant of 4.25 Å, 144 GPa, and 51, respectively. The corresponding experimental data are 4.191 Å, 152 GPa, and 45–47, respectively.[19,20] A good agreement with the experiment is also obtained in the case of the face-centered-cubic (fcc) phase of both Pd and Ni. Further technical details and the full list of calculations and results obtained in this study are reported and discussed in the ESI.†

To investigate reaction (1), we first consider a hydrogen species far from a TPB, on the surface and in the bulk of both the metal and electrolyte components. To calculate the energy of hydrogen,[21] we use:

$$\Delta E_H^q = E_0(H,q) - E_0 - \mu_H + q\varepsilon_f, \qquad (2)$$

where $E_0(H,q)$ is the total energy of the defective material including hydrogen in the charged state q, E_0 is the total energy of the undefective system, and μ_H and ε_f are the chemical potentials for hydrogen and electrons, respectively. In this study, we use a μ_H equal to half the energy of H_2. The value of ε_f in the electrolyte is assumed to lie at the mid-gap, while in both Ni and Pd hydrogen is present in the form of a screened proton, ΔE_H^0 and ΔE_H^+ are found to be equal, and specifying ε_f is not necessary. Further details about the calculation of proton formation energies *via* (2) are reported in the ESI.†

Results and discussion

Our DFT calculations show that the most stable form of hydrogen in BZY is a proton bonded to a lattice oxygen ion, forming the so-called protonic species.[22] In $BaZrO_3$ (BZ), the O–H bond is found to lie in one of the equivalent {100} planes of the ideal perovskite structure, and the energy obtained by using eqn (2) is 0.54 eV (Fig. 1). In lightly Y-doped BZY, our calculations based on the use of model structures of $BaZr_{1-x}Y_xO_3$ with x up to 0.074 show that the defect energy undergoes a significant change only when the protonic species lies within the first coordination shell of a Y dopant (Fig. 1). In such configurations, the defect energy drops to about 0.15 when the protonic species is in contact with two Y dopants, and to 0.35 eV when only one Y lies within the first coordination shell of the protonic species (Fig. 1).

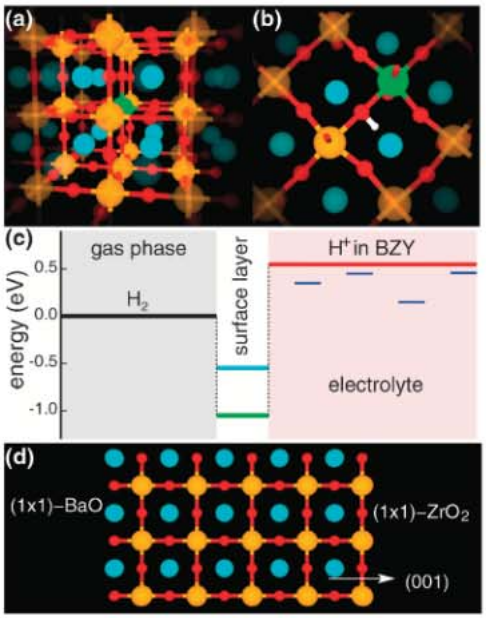

Fig. 1 (a) Ball-and-stick illustration of a substitutional Y-dopant in $BaZrO_3$. (b) A protonic species in contact with a Y dopant in BZY. (c) Energy scheme derived from DFT of a proton in BZY. The red colored line indicates the energy of H^+ in the bulk of BZ. Blue colored segments show the energy of protonic species in contact with Y dopants in BZY. Cyan and green colored segments show the energy of a protonic species at the BaO and ZrO_2 terminations of the BZ(001) surface, respectively. (d) Ball-and-stick illustration of the slab model used to compute the energy of H^+ at the terminations of the BZ(001) surface. Ba, Zr, O, Y, and H atoms are shown in cyan, orange, red, green, and white colors, respectively.

On the surface of BZY, water vapor reacts with oxygen vacancies yielding hydroxide ions and protons.[22] In PCFCs, this process occurs in the cathode, and in the reverse direction, while in the anode protons are supplied by the metal particles and reach the electrolyte surface by crossing TPBs. In the bulk of BZY, the transport of protonic defects occurs *via* rotational diffusion followed by proton transfer between next-nearest neighboring oxygen ions.[22] The migration process of protons in BZY has been recently addressed both experimentally[22,23] and computationally.[24–27] Our results above agree with those reported in recent computational studies.[24–28]

Our calculations show that on the surface of BZY H^+ forms a very stable protonic species. In these calculations, we consider the thermodynamically stable[29] and apolar BZ(001) surface, and a H^+ at both its BaO and ZrO_2 terminations (Fig. 2). In particular, we find that the energy of H^+ at the BaO and ZrO_2 terminations is equal to −0.55 eV and −1.05 eV, respectively (see ESI† for additional details). These energies are considerably lower than the bulk energy value of 0.54 eV, showing that protonic species require to overcome energy barriers larger than 1.1–1.6 eV to escape the free surface and incorporate into the bulk of BZY. Notably, our calculations show that, on both terminations, H^+ recovers the bulk energy value after penetrating the three topmost superficial (001) layers (Fig. 2).

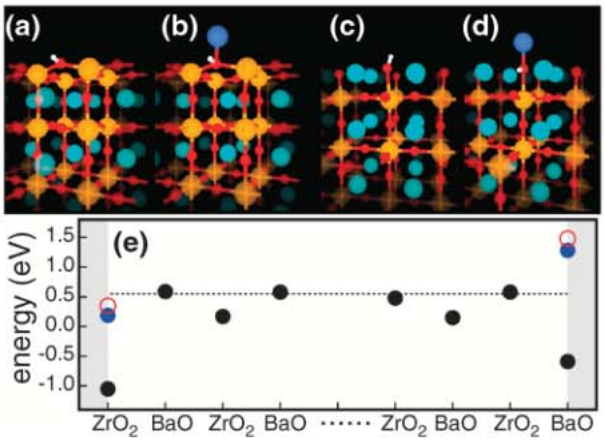

Fig. 2 (a) Ball-and-stick illustration of a protonic species at the ZrO_2 termination of the BZ(001) surface. (b) The same protonic defect in contact with a Pd atom adsorbed on the surface. (c) and (d) show similar configurations of a protonic species on the BaO termination of the BZ(001) surface. Ba, Zr, O, Pd, and H atoms are shown in cyan, orange, red, blue, and white colors, respectively. (e) Energy of a protonic defect at surface layers near the BaO and ZrO_2 terminations of the BZ(001) surface. The vacuum is indicated by gray areas. Red and blue symbols show the energy of the protonic species in contact with a Pd and Ni atom, respectively.

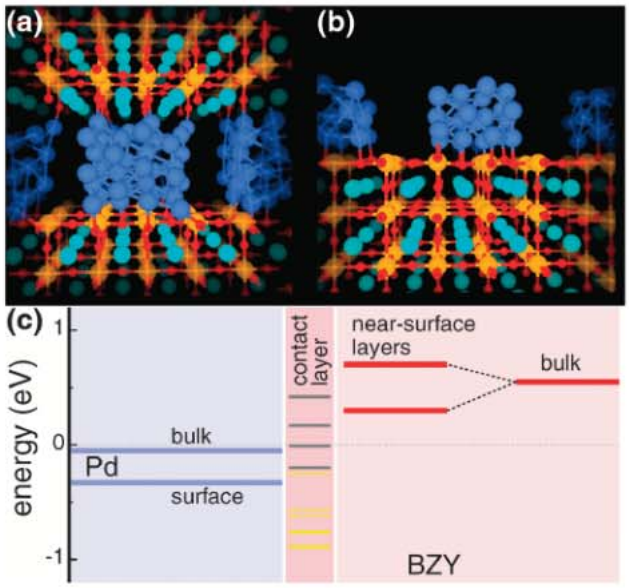

Fig. 3 (a) A 48-atom Pd cluster sandwiched between the ZrO_2 and BaO terminations of the BZ(001) surface. (b) A 24-atom Pd cluster in contact with the ZrO_2 termination of the slab model. Ba, Zr, O, and Pd atoms are shown in cyan, orange, red, and blue colors, respectively. (c) Energy diagram of a hydrogen species crossing TPBs based on Pd and BZ. Colored areas identify the key regions of the TPBs: the metal catalyst in light blue, the surface layer of BZ in contact with the metallic and gas phases in salmon color, and the sub-surface and bulk regions of BZ in pink. The colored segments show the energy of hydrogen in these regions. From left to right, hydrogen on the (111) surface and in the bulk of Pd, at the BZ(001) layer in contact with Pd and vacuum, in the near-surface region of the electrolyte beneath the topmost surface layer, and in the bulk of BZY. Full and dashed yellow segments indicate the energy of H^+ at peripheral sites of the metal–electrolyte interface in full and partial contact with metallic ions, respectively. Gray segments show the energy of protonic species buried beneath the metal cluster.

In the bulk of both Pd and Ni, hydrogen finds stable configurations corresponding to the octahedral (O_h) and tetrahedral (T_d) sites of the fcc lattice.[30] Our calculations give, in particular, energies of −0.02 eV and 0 eV for a hydrogen species in Pd at the O_h and T_d sites, respectively. In bulk Ni, these energy values are 0.16 eV and 0.42 eV, respectively. On the surface of both Pd and Ni, hydrogen finds solubility sites at lower energy. In the case of the Pd(111) and Ni(111) surfaces, we obtained defect energies of about −0.33 eV and −0.47 eV, respectively (ESI†). In accord with the experiment, these results suggest that hydrogen species resulting from the dissociation of H_2 reach the TPBs by diffusing into the near-surface region of these metallic catalysts. To enter into the bulk of Pd and Ni, the results above show that hydrogen needs to overcome an energy step of about 0.35 eV and 0.63 eV, respectively.

Reaction (1) occurs at the TPB, near the metal–electrolyte interface. To address the chemical effects, we consider a single metal atom adsorbed on the BZ(001) surface, and we compute the energy of a superficial proton in direct contact with the metal atom (Fig. 2). DFT calculations show that, in contact with either Pd or Ni, the energy of the interfacial proton increases up to, and in the case of BaO terminations even beyond, the energy value that H^+ assumes in the bulk of BZY (Fig. 2). In detail, upon the ZrO_2 termination the proton energy increases by about 1.3 eV, while upon the BaO termination it raises by about 2 eV.

To address reaction (1), we consider three realistic model structures of TPBs based on BZY (Fig. 3 and 4). In these models, the electrolyte is represented by a slab consisting of 3 × 3 × 3 primitive unit cells of perfect BZ, *i.e.* devoid of Y dopants and oxygen vacancies, while the metal catalyst is modeled through the use of a cluster. In a first case, for both Pd and Ni we use a 48-atom metal cluster sandwiched between the two terminations of the slab. In the case of Pd only, we further consider the case of a 24-Pd cluster adsorbed on the ZrO_2 termination of the BZ(001) slab. These models are used to calculate the energy of final states for reaction (1), *i.e.* a proton in the electrolyte component of the TPB and an electron added to the metal cluster. In all cases, this is achieved by inserting a neutral hydrogen atom in the BZ slab near an O ion, and by performing a full structural optimization of the defective structure. A Bader charge analysis[31] confirms that, in all cases, hydrogen is positively charged and an additional electron resides on the metal cluster.

Our results show that, regardless of the nature of the metal component, the energy of protons in the electrolyte near the TPB exhibits well-defined behaviors (see ESI† for details). Protons at the terminal layer of the electrolyte assume variable energies, depending on the local chemical environment. In agreement with the results in Fig. 2, protonic species buried underneath the metal cluster attain, in particular, the largest energy values, up to that of H^+ in the bulk of BZY, while at peripheral sites of the metal particle, they assume low energies, close to that of hydrogen on the (111) surface of the catalyst (Fig. 3 and 4). In the sub-surface layers of the electrolyte, beneath the layer in contact with the metal and the gas phase, the proton assumes, on the other hand, a nearly constant value,

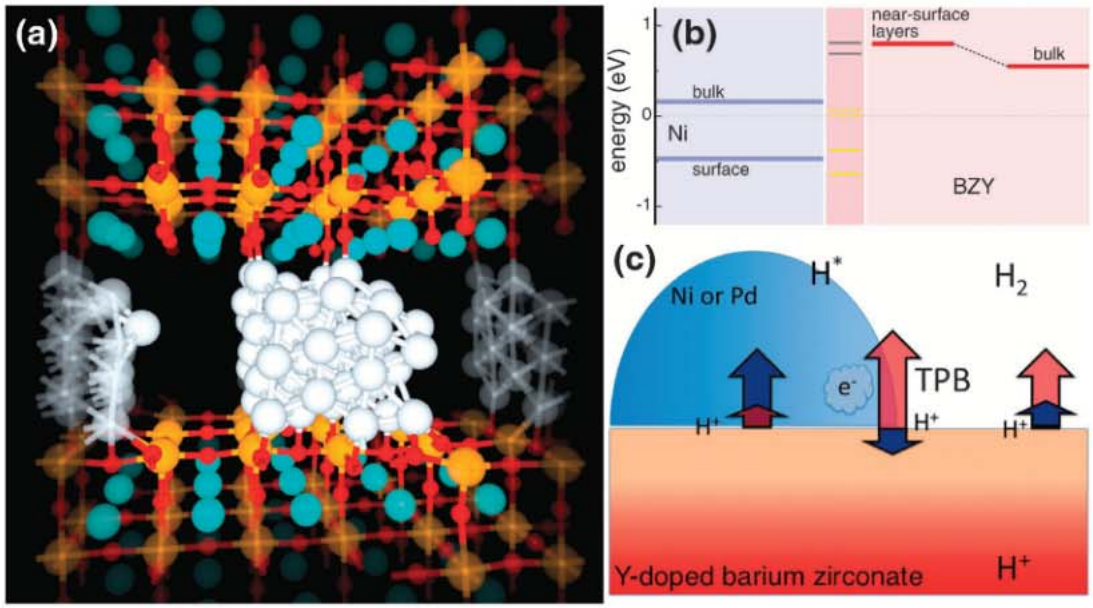

Fig. 4 (a) A 48-atom Ni cluster sandwiched between the terminations of the BZ(001) surface. Ba, Zr, O, and Ni atoms are shown in cyan, orange, red, and white colors, respectively. (b) Energy diagram of a hydrogen species crossing TPBs based on Ni and BZ. Colored areas and segments have the same meaning as in Fig. 3. (c) Schematic of a TPB based on BZY sketching the energies involved in reaction (1) occurring, from left to right, at buried regions of the metal–electrolyte interface, peripheral sites of the interface, and far from the TPB on the surface of the electrolyte. Blue arrows indicate the energies of protonic species at these regions, while red arrows are used to indicate the energy cost to incorporate the electrolyte.

shifted by ΔE with respect to the energy of H^+ in the bulk of BZY (Fig. 3 and 4). To rationalize the values obtained for ΔE, we calculate the Schottky barrier height (E_{SBH}) at the metal–electrolyte contacts of the TPB models shown in Fig. 3 and 4. These calculations show that ΔE satisfies the following simple relation:

$$\Delta E = \varepsilon_f^{BZY} - (\varepsilon_v + E_{SBH}), \quad (3)$$

where ε_f^{BZY} is the Fermi energy lying at the mid-gap in the bulk of BZY and ε_v is the maximum of the valence band of BZY. The energy values for E_{SBH} are 1.3 eV, 1.7 eV, and 1.9 eV for the Pd–BZ and Ni–BZ interfaces shown in Fig. 3(a), (b) and 4, respectively.

Conclusions

The main findings of this study are summarized by the equilibrium energy diagrams shown in Fig. 1, 3 and 4. These energy schemes show that reaction (1) – that is the key transfer process of a hydrogen species from a metal catalyst to the electrolyte at a TPB – involves two critical steps: hydrogen spilling onto the electrolyte surface and proton penetration of the near-surface layers in proximity of the metal–electrolyte contact. Reaching, spilling, and incorporating the electrolyte at buried regions of the metal–electrolyte interface correspond to a sequence of endothermic steps, involving energy costs around 0.3–0.7 eV. The overall process is energetically uphill. Reaching and spilling at peripheral sites of the metal–electrolyte interface at the TPB correspond, on the other hand, to exothermic steps whose kinetics is controlled only by migrational barriers. At these sites, however, the protons find highly stable energy traps on the electrolyte surface, and the incorporation process involves energy costs larger than 1 eV. Similar energy costs are also required to penetrate the terminal layer of the electrolyte, far from the TPB and in contact with the gas phase. To reach these surface sites, however, the protons need to escape the trap states at the TPB and migrate toward the free surface.

Overall, this work shows that the proton-transfer resistance at TPBs based on BZY is a property controlled by the terminal surface layer of the electrolyte in contact with the metallic and gas phases. In agreement with recent findings,[5,6] hydrogen spilling onto the electrolyte surface is favored at peripheral sites of the metal–electrolyte interface. However, penetration and migration across this surface layer involve energies of the order of 1 eV, sufficiently large to influence the kinetics of the whole fuel cell anode. In proximity of TPBs, the energy costs associated with reaction (1) are controlled by the nature of the electrolyte, metal catalyst, and also their chemical and Schottky contact. This basic understanding may be key to advance fuel cell, hydrogen separation, and electrolyzer technologies.

Acknowledgements

The authors acknowledge the support of the Samsung Advanced Institute of Technology (SAIT). M.M. and A.B. also acknowledge the support of the NSF grant CHE-0946869.

References

1 B. C. H. Steele, *J. Mater. Sci.*, 2001, 36, 1053.
2 J. Mukherjee and S. Linic, *J. Electrochem. Soc.*, 2007, 154, B919.

3 M. Vogler, A. Bieberle-Hütter, L. Gauckler, J. Warnatz and W. Bessler, *J. Electrochem. Soc.*, 2009, 156, B633.
4 D. G. Goodwin, H. Zhu, A. Colclasure and R. Keeb, *J. Electrochem. Soc.*, 2009, 156, 1004.
5 M. Shishkin and T. Ziegler, *J. Phys. Chem. C*, 2009, 113, 21667.
6 C. S. Cucinotta, M. Bernasconi and M. Parrinello, *Phys. Rev. Lett.*, 2011, 107, 206103.
7 E. Fabbri, D. Pergolesi and E. Traversa, *Chem. Soc. Rev.*, 2010, 39, 4355.
8 F. Lefebvre-Joud, G. Gauthier and J. Mougin, *J. Appl. Electrochem.*, 2009, 39, 535.
9 H. Zhu, R. J. Kee, V. M. Janardhanan, O. Deutschmann and D. G. Goodwin, *J. Electrochem. Soc.*, 2005, 152, A2427.
10 J. R. Wilson, W. Kobsiriphat, R. Mendoza, H.-Y. Chen, J. M. Hiller, D. J. Miller, K. Thornton, P. W. Voorhees, S. B. Adler and S. A. Barnett, *Nat. Mater.*, 2006, 5, 541.
11 J. Ruiz-Morales, J. Canales-V'azquez, C. Savaniu, D. Marrero-López, W. Zhou and J. Irvine, *Nature*, 2006, 439, 568.
12 M. L. Liu, M. E. Lynch, K. Blinn, F. M. Alamgir and Y. Choi, *Mater. Today*, 2011, 14, 844.
13 M. Shishkin and T. Ziegler, *J. Phys. Chem. C*, 2008, 112, 19662.
14 L. Yang, S. Wang, K. Blinn, M. Liu, Z. Liu, Z. Cheng and M. Liu, *Science*, 2009, 326, 126.
15 L. Yang, Y. Choi, W. Qin, H. Chen, K. Blinn, M. Liu, P. Liu, J. Bai, T. A. Tyson and M. L. Liu, *Nat. Commun.*, 2011, 2, 357.
16 D. Pergolesi, E. Fabbri, A. D'Epifanio, E. D. Bartolomeo, A. Tebano, S. Sanna, S. Licoccia, G. Balestrino and E. Traversa, *Nat. Mater.*, 2010, 9, 846.
17 G. Kresse and J. Furthmüller, *Comput. Mater. Sci.*, 1996, 6, 15.
18 G. Kresse and J. Furthmüller, *Phys. Rev. B: Condens. Matter Mater. Phys.*, 1996, 54, 11169.
19 A. R. Akbarzadeh, I. Kornev, C. Malibert, L. Bellaiche and J. M. Kiat, *Phys. Rev. B: Condens. Matter Mater. Phys.*, 2005, 72, 205104.
20 K. Goretta, E. Park, R. Koritala, M. Cuber, E. Pascual, N. Chen, A. de Arellano-López and J. Routbort, *Physica C*, 1998, 309, 245.
21 C. G. V. de Walle and J. Neugebauer, *Nature*, 2003, 423, 626.
22 K. D. Kreuer, *Annu. Rev. Mater. Res.*, 2003, 33, 333.
23 K. D. Kreuer, *Solid State Ionics*, 1999, 125, 285.
24 P. G. Sundell, M. E. Björketun and G. Wahnström, *Phys. Rev. B: Condens. Matter Mater. Phys.*, 2007, 76, 094301.
25 Q. Zhang, G. Wahnström, M. E. Björketun, S. Gao and E. Wang, *Phys. Rev. Lett.*, 2008, 101, 215902.
26 B. Merinov and W. Goddard III, *J. Chem. Phys.*, 2009, 130, 194707.
27 P. Raiteri, J. D. Gale and G. Bussi, *J. Phys.: Condens. Matter*, 2011, 23, 334213.
28 M. A. Gomez, M. Chunduru, L. Chigweshe, L. Foster, S. J. Fensin, K. M. Fletcher and L. E. Fernandez, *Appl. Phys. Lett.*, 2010, 132, 214709.
29 N. Iles, F. Finocchi and K. D. Khodja, *J. Phys.: Condens. Matter*, 2010, 22, 305001.
30 S. Xu, P. Sood, M. Liu and A. Bongiorno, *Appl. Phys. Lett.*, 2011, 99, 181901.
31 W. Tang, E. Sanville and G. Henkelman, *J. Phys.: Condens. Mater.*, 2009, 21, 084204.